J. Fluid Mech. (1995), vol. 283, pp. 249–272

Primary and secondary instabilities of the asymptotic suction boundary layer on a curved plate

By DANIEL S. PARK† AND PATRICK HUERRE‡
Department of Aerospace Engineering, University of Southern California, Los Angeles, CA 90089-1191, USA

(Received 19 April 1991 and in revised form 24 June 1994)

The temporal growth of Görtler vortices and the associated secondary instability mechanisms are investigated numerically in the case of an asymptotic suction boundary layer on a curved plate. Highly inflectional velocity profiles are generated in both the spanwise and vertical directions. The inflectional velocity profile develops earlier in the spanwise direction. There exist two distinct modes of instability that eventually lead to the breakdown of Görtler vortices: the sinuous mode and the varicose mode. The temporal secondary instability analysis of the three-dimensional inflectional velocity profile reveals that the sinuous mode becomes unstable earlier than the varicose mode. The sinuous mode is shown to be primarily related to shear in the spanwise direction, $\partial U/\partial z$, and the varicose mode to shear in the vertical direction, $\partial U/\partial y$.

1. Introduction

For nearly a century, hydrodynamic stability and transition have been recognized as a central problem of fluid mechanics. Understanding of laminar–turbulent transition is very crucial and essential to the improvement of modern technology. Flow over a concave wall, known as Görtler flow, is susceptible to a centrifugal instability due to the streamline curvature. Counter-rotating streamwise vortex pairs are created when the radial pressure gradient can no longer balance the centrifugal force as shown schematically in figure 1. The presence of such vortices is important in flows over a turbine blade or on the lower surface of airfoils since streamwise vortices can drastically change the heat transfer rate and the skin friction characteristics.

Rayleigh (1916), using an inviscid analysis, derived a simple condition for the occurrence of an instability with respect to rotationally symmetric disturbances. This condition, known as the Rayleigh circulation criterion for the stability of an inviscid fluid, states that, if the circulation decreases in the radial direction, the flow is inviscidly unstable. According to this theory, the boundary layer over a concave wall is unstable on inviscid grounds. Görtler (1940) then deduced theoretically that the effect of the centrifugal force due to the streamline curvature of the boundary layer gives rise to the formation of streamwise vortices. This mechanism is analogous to the Taylor–Couette flow instability investigated by Taylor (1923). The Görtler number G as first

† Present address: Naval Command, Control and Ocean Surveillance Center, RDT&E Division, Code 574, San Diego, CA 92152-6040, USA.
‡ Present address: Laboratoire d'Hydrodynamique (LADHYX), Ecole Polytechnique, 91128 Palaiseau Cedex, France.

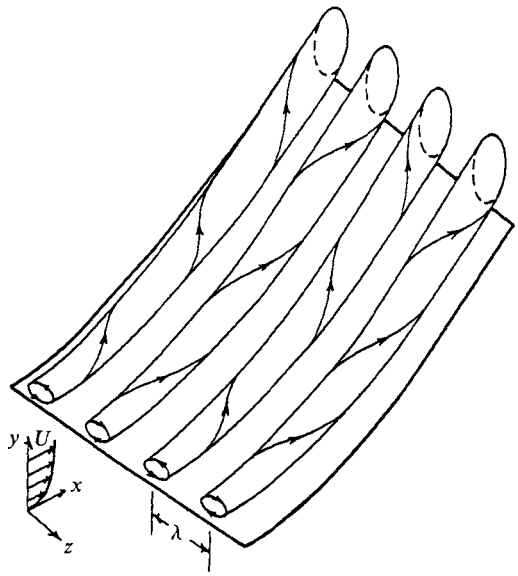

FIGURE 1. Sketch of the streamwise vortices developing on a concave wall due to the Görtler instability (from Swearingen & Blackwelder 1987).

formulated by Görtler (1940) is the most important parameter in this problem and it is defined by

$$G = R_E(\theta/R)^{1/2}, \tag{1}$$

where R_E is the Reynolds number based on the free-stream velocity U_∞ and the momentum thickness θ of the boundary layer and R is the radius of curvature of the wall. Peerhosaini (1984) showed that the Görtler number is essentially the ratio of a stabilizing timescale due to viscous diffusion and a destabilizing timescale due to the centrifugal force. Therefore, when the Görtler number exceeds a critial value G_c, the flow becomes unstable.

It is appropriate to briefly discuss relevant experimental and theoretical results concerning the growth and the breakdown of Görtler vortices. Bippes (1972) produced an isotropic field of disturbances with screens in the oncoming flow. Out of the entire spectrum of disturbances, only those corresponding to the longitudinal vortex component at a certain wavelength were excited. His hydroden bubble visualizations reveal that the vortices grow, meander and, then, break down. Aihara (1979) and Winoto & Crane (1980) observe low-frequency vortex meandering in the spanwise direction and Aihara & Koyama (1981) suggest that this meandering motion may result from the production of a normal component of vorticity. Ito (1980) also reports a low-frequency motion before the appearance of the horseshoe-type vortices.

Görtler vortices in spatially growing boundary layers have been extensively studied analytically by Hall and his co-workers. Hall (1982*b*, 1983) has emphasized that it is not legitimate to consider the basic velocity profile as locally parallel unless one restricts attention to the high-wavenumber limit. This peculiar situation seriously complicates the analytical investigation of the Görtler instability. Considerable progress has been made nonetheless: the nonlinear spatial evolution of Görtler vortices at high wavenumbers has been described analytically in the weakly nonlinear regime by Hall (1982*a*) and in the strongly nonlinear regime by Hall & Lakin (1988). The corresponding numerical study for arbitrary wavenumbers has been performed by Hall

(1988). One of the salient features of these analyses is that the dominant nonlinear effect involves a strong interaction between the mean flow and the fundamental. Moreover, the downstream flow development leads to the formation of highly inflectional velocity profiles that could support rapidly growing inviscid modes of instability. According to classical instability theory, two-dimensional inflectional profiles are unstable to wavelengths of the same order as the shear layer thickness, their growth rate being much larger than in the case of viscous Tollmien–Schlichting-type instabilities. The emergence of an inflectional velocity profile has been carefully documented in the experiments of Swearingen & Blackwelder (1987). In particular, these investigations demonstrated that time-dependent fluctuations appearing in the flow are more closely correlated with shear in the spanwise direction than in the vertical direction. This observation is at variance with the idea that breakdown first takes place in the region of high inflectional shear in the vertical direction. The same phenomena are also prominent in the recent numerical investigation of temporally evolving Görtler vortices performed by Sabry & Liu (1991) and in direct numerical simulations of transition to turbulence in Görtler flow by Liu & Domaradzki (1990) and Liu (1991).

The secondary instabilities arising on the primary Görtler vortices have only recently been examined theoretically. Hall & Seddougui (1989) and Bassom & Seddougui (1990) have shown that, in the high-wavenumber limit, Görtler vortices can support neutrally stable three-dimensional disturbances giving rise to wavy vortex boundaries. However, the secondary inviscid instabilities associated with the development of inflectional profiles in the spanwise and vertical directions appear to be the most likely sources of strongly amplified three-dimensional disturbances. Their study is one of the main objectives of this paper.

Part of our analysis is conducted in the same spirit as the recent study by Hall & Horseman (1991) on the linear secondary instability properties of longitudinal vortex structures in boundary layers.† These authors derive the counterpart of the usual Rayleigh equation for a class of three-dimensional spatially periodic flows consisting of streamwise vortices. They demonstrate that such flows can give rise to amplified secondary perturbations. Their work will be referred to during the course of the discussion.

The first goal of our study is to document numerically the nonlinear temporal growth of the primary Görtler vortices arising on a concave wall which, prior to instability onset, supports an asymptotic suction boundary layer. This particular configuration has been deliberately chosen so as to obtain a basic flow that is independent of the streamwise distance along the curved wall at leading order in the small parameter θ/R. In this manner, the issue of non-parallelism raised by Hall (1982*b*) does not arise and the problem is well-posed. It cannot be claimed that the situation is identical to the usual Görtler flow in a growing boundary layer, but it is felt that the main features of the instability evolution have been preserved. The second and more important objective of the study is to determine the secondary linear instability properties of the resulting temporally evolving Görtler vortices. Instead of solving an eigenvalue problem as in Hall & Horseman (1991) we have chosen to integrate numerically the Navier–Stokes equations linearized about the time-dependent Görtler state. In this procedure, we take advantage of the fact that the secondary instability timescale is much shorter than the Görtler evolution timescale. The Görtler evolution time can therefore be legitimately used as a parameter. The secondary instability properties are determined, at various stages of the Görtler vortex growth, by examining

† The present paper was being prepared while the study of Hall & Horseman (1991) appeared in this journal.

the long-time exponential behaviour of the solutions of the linearized Navier–Stokes equations.

2. Problem formulation

Consider flow over a concave wall with constant radius of curvature R, the free-stream velocity being U_∞ and the kinematic viscosity of the fluid being ν. The Reynolds number based on the momentum thickness θ of the undisturbed asymptotic suction boundary layer is defined as

$$R_E = U_\infty \theta/\nu. \tag{2}$$

We choose dimensionless space variables x, y, z (see figure 1) scaled with respect to θ and a dimensionless time variable t scaled with respect to θ/U_∞. The velocity components U, V, W and pressure field P for the basic flow as well as corresponding quantities u, v, w and p for the disturbance field are made dimensionless with the velocity scale U_∞ and the dynamic pressure ρU_∞^2, where ρ denotes the density of the fluid.

The basic flow is assumed to be composed of the asymptotic suction boundary layer and temporally growing Görtler vortices. Its velocity and pressure fields are defined as follows:

$$U = 1 - e^{-0.5y} + U_g(y, z, T), \tag{3}$$

$$V = R_E^{-1}\{-0.5 + V_g(y, z, T)\}, \tag{4}$$

$$W = R_E^{-1} W_g(y, z, T), \tag{5}$$

$$P = R_E^{-2}\{P_B(y) + P_g(y, z, T)\}, \tag{6}$$

where $P_B(y)$ is the pressure field that balances the centrifugal effect. Note that Görtler vortices evolve on the slow time variable $T = R_E^{-1} t$. The Görtler field quantities are obtained by solving the following nonlinear partial differential equations:

$$\frac{\partial U_g}{\partial T} + (U_g \cdot \nabla_g) U_g + \frac{dU_B}{dy} V_g - 0.5 \frac{\partial U_g}{\partial y} = \frac{\partial^2 U_g}{\partial y^2} + \frac{\partial^2 U_g}{\partial z^2}, \tag{7}$$

$$\frac{\partial V_g}{\partial T} + (U_g \cdot \nabla_g) V_g - 0.5 \frac{\partial V_g}{\partial y} + G^2(2U_B U_g + U_g^2) = -\frac{\partial P_g}{\partial y} + \frac{\partial^2 V_g}{\partial y^2} + \frac{\partial^2 V_g}{\partial z^2}, \tag{8}$$

$$\frac{\partial W_g}{\partial T} + (U_g \cdot \nabla_g) W_g - 0.5 \frac{\partial W_g}{\partial y} = -\frac{\partial P_g}{\partial z} + \frac{\partial^2 W_g}{\partial y^2} + \frac{\partial^2 W_g}{\partial z^2}, \tag{9}$$

$$\frac{\partial V_g}{\partial y} + \frac{\partial W_g}{\partial z} = 0, \tag{10}$$

where

$$U_g \cdot \nabla_g = V_g \frac{\partial}{\partial y} + W_g \frac{\partial}{\partial z}, \tag{11}$$

and $U_B(y)$ represents the asymptotic suction velocity profile introduced in (3). The associated boundary conditions are

$$U_g = V_g = W_g = 0 \quad \text{at} \quad y = 0, \infty. \tag{12}$$

The derivation of these equations in the limit of $R_E \gg 1$, $\theta/R \ll 1$, $G = O(1)$, and the justification for the choice of scales is given in Hall (1982*a*) and Floryan & Saric (1979).

We wish to consider the linear stability of the Görtler flow defined above with respect to infinitesimal three-dimensional disturbances evolving on the fast timescale t and

characterized by a velocity field $\boldsymbol{u}(x, y, z, t)$ and a pressure field $p(x, y, z, t)$. The equations to be solved are the Navier–Stokes equations linearized about the basic state $U(y, z, T) = (U, V, W)$ and $P(y, z, T)$:

$$\frac{\partial \boldsymbol{u}}{\partial t} + (\boldsymbol{U}\cdot\boldsymbol{\nabla})\,\boldsymbol{u} + (\boldsymbol{u}\cdot\boldsymbol{\nabla})\,\boldsymbol{U} = -\boldsymbol{\nabla}p + \frac{1}{R_E}\nabla^2\boldsymbol{u}, \tag{13}$$

$$\boldsymbol{\nabla}\cdot\boldsymbol{u} = 0, \tag{14}$$

where $\boldsymbol{u} = (u, v, w)$ and the associated boundary conditions are

$$u = v = w = 0 \quad \text{at} \quad y = 0, \infty. \tag{15}$$

It must be emphasized that the slow time variable T only appears as a parameter in the above system. This is because the Görtler evolution time scale is $\tau_g \sim \theta^2/\nu$, whereas the expected evolution timescale of the secondary inflectional instability is $\tau_i \sim \theta/U_\infty$. Thus

$$\tau_i/\tau_g \sim R_E^{-1} \ll 1, \tag{16}$$

which is strictly equivalent to the relation $T = R_E^{-1}\,t$ between the Görtler time variable T and the inflectional instability variable t. In the secondary instability analysis, it is therefore justified to consider the basic Görtler flow as quasi-steady and to treat T as a parameter. The Reynolds number R_E will be chosen to be 1000, which is well below the critical Reynolds number for the onset of a viscous Tollmien–Schlichting instability in the asymptotic suction boundary layer (Drazin & Reid 1981). Therefore, if instabilities are present, it is clear that they do not originate from a viscous instability mechanism.

The basic flow possesses the following invariance properties in the spanwise direction:

$$(z, U, V, W) \rightarrow (-z, U, V, -W). \tag{17}$$

From this, one can easily see that there are two independent instability modes. The first one is the sinuous mode, which has the following invariance properties:

$$(z, u, v, w, p) \rightarrow (-z, -u, -v, w, -p). \tag{18}$$

The second one is the varicose mode which has the following invariance properties:

$$(z, u, v, w, p) \rightarrow (-z, u, v, -w, p). \tag{19}$$

3. Numerical method

The time-dependent Görtler equations (7)–(11) are solved by means of a pseudo-spectral scheme whereby the variables U_g, V_g, W_g and P_g are expanded into finite Fourier series in the spanwise direction so that

$$(U_g, V_g, P_g) = \sum_{m=0}^{M} \{U_m(y, T), V_m(y, T), P_m(y, T)\} \cos mk_z z, \tag{20}$$

$$W_g = \sum_{m=0}^{M} W_m(y, T) \sin mk_z z. \tag{21}$$

An exponentially stretched grid is generated in the vertical y-direction so as to accommodate high gradients near the wall. This is achieved by introducing the exponential mapping

$$\eta = \frac{1 - \mathrm{e}^{-\alpha y}}{1 - \mathrm{e}^{-\alpha y_\infty}}, \tag{22}$$

where $\alpha = 0.04$, $y_\infty = 200$. With this choice of parameter values, 33 % of the grid points lie within a boundary layer thickness. Temporal evolution over an interval of time ΔT

G	k_z	σ_{100}	σ_{200}	σ_{lin}
5	0.5	0.9044	0.9020	0.9027
8	0.5	1.7653	1.7611	1.7633
10	0.5	2.3483	2.3429	2.3463
5	0.8	0.7553	0.7533	0.7530
8	0.8	1.7751	1.7793	1.7811
10	0.8	2.4682	2.4736	2.4771

TABLE 1. Comparison between computed primary instability growth rates σ_{100} and σ_{200} for 100 and 200 grid points in the y-direction respectively and growth rates σ_{lin} predicted from the linear stability eigenvalue problem, for different Görtler numbers G and spanwise wavenumbers k_z

is accomplished in three steps. The first one is a nonlinear step which accounts for the effects of curvature and the convective terms. The second one is a pressure step associated with the pressure gradient terms and where the divergence-free condition is applied. The final updated values at time $T+\Delta T$ are then obtained in a third implicit viscous step in which the viscous diffusion terms are calculated and the no-slip condition is enforced.

Extensive numerical resolution studies have been performed to test the accuracy of the numerical scheme. In table 1, the computed growth rates σ_{100} and σ_{200} pertaining to 100 and 200 grid points in the y-direction are compared, for different Görtler numbers G and spanwise wavenumbers k_z, to the growth rates σ_{lin} predicted by solving the linear stability eigenvalue problem. The number of Fourier modes M and the time step ΔT are held fixed at $M = 16$ and $\Delta T = 0.01$. Doubling the number of grid points in the y-direction is seen to change the growth rates by only 0.2%. We note that the initial growth rate is not sensitive to the number of spanwise Fourier modes M since most of the perturbation energy is contained in the fundamental mode. To access the effect of varying M, it is more meaningful to compare the results obtained in the nonlinear regime: when M is doubled from 16 to 32, the total perturbation energy contained in the Görtler vortices in the fully saturated nonlinear stage merely changes from 1.071477×10^{-3} to 1.071484×10^{-3}. On the basis of these comparative studies, the number of grid points in the y-direction and the number of Fourier modes have been held fixed at 100 and 16 respectively, in all the computational results presented in this paper.

In order to solve the secondary instability equations (13) and (14), one takes advantage of the invariance properties mentioned in the previous section. Sinuous perturbations of streamwise wavenumber k_x are expanded into the following Fourier series:

$$(u, v, p) = e^{ik_x x} \sum_{m=0}^{M} \{u_m(y,t), v_m(y,t), p_m(y,t)\} \sin mk_z z + \text{c.c.}, \tag{23}$$

$$w = e^{ik_x x} \sum_{m=0}^{M} w_m(y,t) \cos mk_z z + \text{c.c.}, \tag{24}$$

where it is assumed that periodicity holds in the spanwise direction at the same wavenumber k_z as in the basic Görtler flow. Varicose perturbations of streamwise wavenumber k_x admit similar expansions with sine and cosine functions being interchanged. The linear stability equations are solved with the same numerical method used to integrate the Görtler equations for the same value of M. They are numerically integrated until an asymptotic limit of the form $e^{(-i\omega_r+\omega_i)t}$ is established. One can therefore retrieve from this simple procedure the most unstable temporal eigenvalue

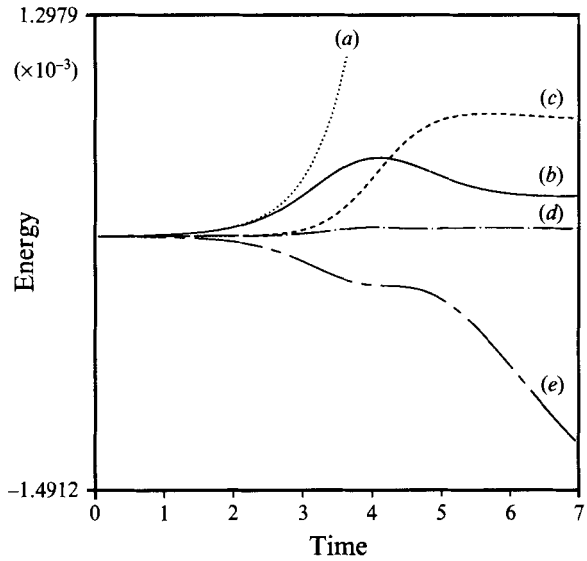

FIGURE 2. Temporal growth of energy for $k_z = 0.5$ and $G = 5$: (*a*) linear theory, (*b*) fundamental, (*c*) mean flow distortion, (*d*) first harmonic, (*e*) mean flow energy at time T minus initial mean flow energy.

Mode type	Δt	Number of Fourier modes	Number of grid points	ω
sinuous	0.1	16	200	0.3197+0.02617i
sinuous	0.2	16	200	0.3194+0.02617i
sinuous	0.2	16	100	0.3195+0.02605i
sinuous	0.3	16	100	0.3297+0.02602i
sinuous	0.2	32	100	0.3195+0.02605i
varicose	0.1	16	200	0.3098+0.02995i
varicose	0.2	16	200	0.3101+0.03007i
varicose	0.2	16	100	0.3089+0.02931i
varicose	0.2	32	100	0.3089+0.02931i

TABLE 2. Sensitivity of computed instability eigenvalue ω with respect to time step Δt, number of Fourier modes M and number of grid points in the y-direction

$\omega = \omega_r + i\omega_i$ and eigenfunction for given values of G, k_z, T and k_x. The numerical accuracy of the secondary instability problem is also checked. As shown in table 2, the temporal eigenvalue ω is virtually unchanged as the number of grid points in the y-direction is doubled from 100 to 200 or the number of Fourier modes M is doubled from 16 to 32. In the following discussion, computational results for the secondary instability are presented with the number of grid points in the y-direction and the number of Fourier modes set at 100 and 16 respectively. The time step has been fixed at $\Delta t = 0.2$.

4. Results and discussion

4.1. *Primary instability*

The Görtler number G chosen in the simulation is 5 and the fundamental spanwise wavenumber k_z is 0.5, which corresponds approximately to the most amplified perturbation at that value of G. The initial condition is taken to be the eigenfunction

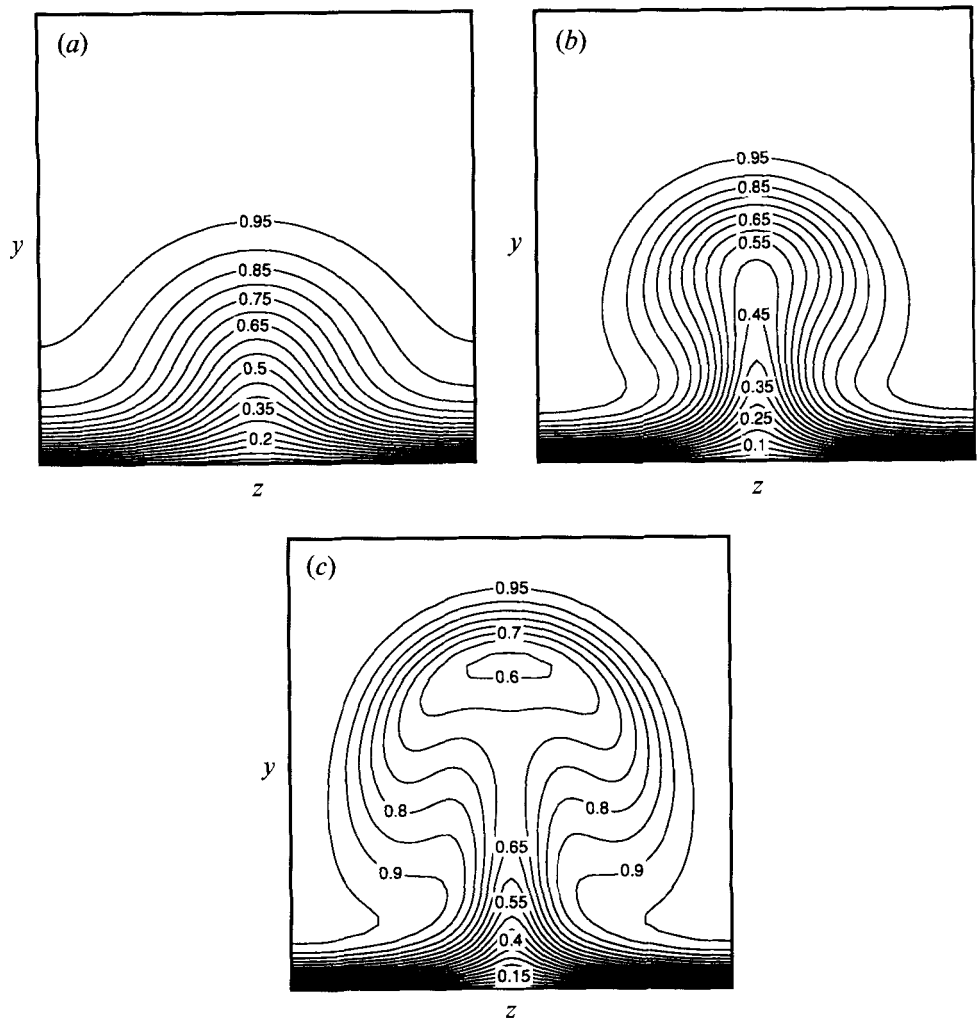

FIGURE 3. Constant streamwise velocity contours in the (y, z)-plane for $k_z = 0.5$ and $G = 5$. (*a*) $T = 3$, (*b*) $T = 4$, (*c*) $T = 5$.

of the linear stability problem, the initial amplitude of the streamwise perturbation being 2% of the free-stream velocity. Figure 2 shows the evolution of the energy e_n in the first three Fourier modes, where e_n is defined by

$$e_0 = \frac{\pi}{k_z}\int_0^\infty U_0^2(y, T)\,\mathrm{d}y, \tag{25}$$

$$e_n = \frac{\pi}{2k_z}\int_0^\infty U_n^2(y, T)\,\mathrm{d}y \quad \text{for} \quad n > 0. \tag{26}$$

The initial growth rate of the vortices agrees with the results given by linear theory as indicated by the dotted line. The energy of the mean flow distortion eventually becomes larger than that of the fundamental. The higher harmonics grow, but most of the energy is contained in the fundamental and the mean flow distortion as emphasized by Hall (1988). One interesting phenomenon is that the energy of the fundamental overshoots its saturated level and later decays down to its saturated state. A similar

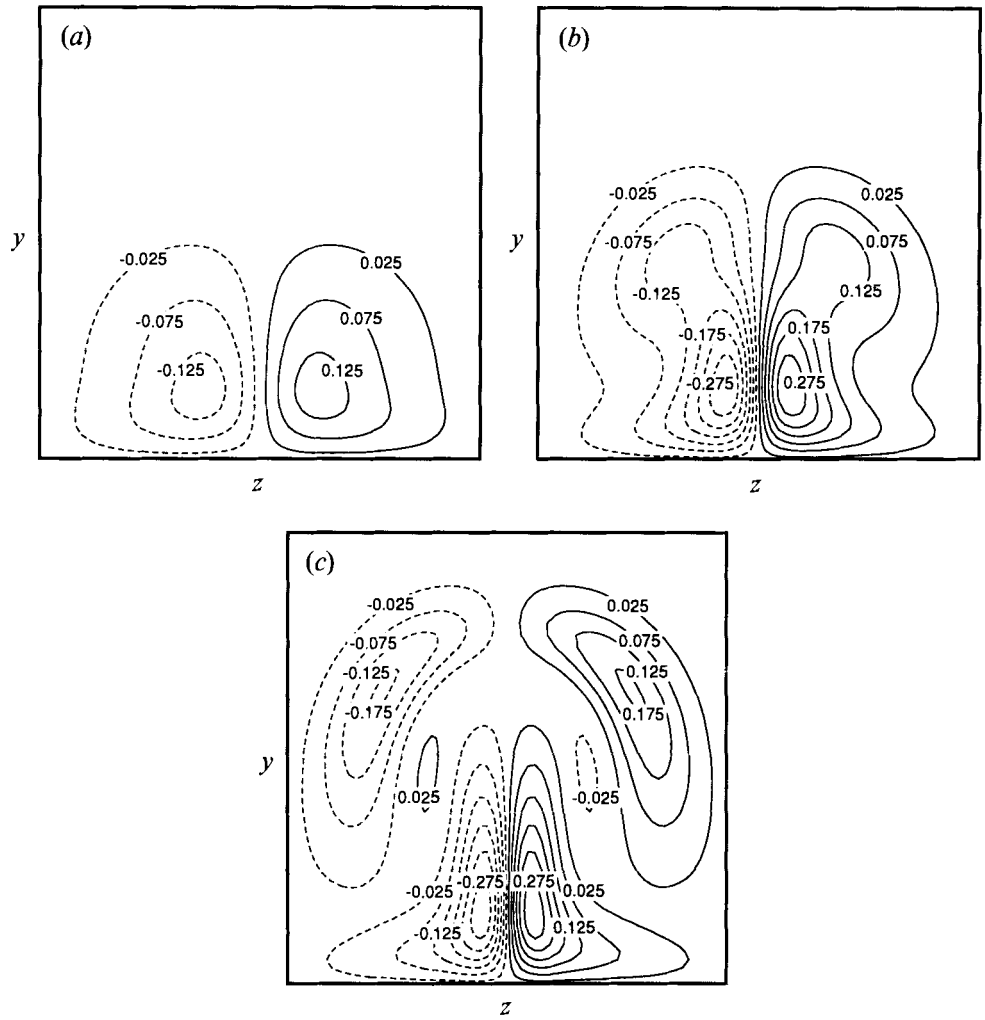

FIGURE 4. Constant $\partial U/\partial z$ contours in the (y, z)-plane for $k_z = 0.5$ and $G = 5$. (*a*) $T = 3$, (*b*) $T = 4$, (*c*) $T = 5$.

behaviour has been observed in the rotating channel flow experiment of Alfredsson & Matsson (1990). The chain-dashed line represents the energy of the mean flow at time T minus the initial mean flow energy of the asymptotic suction velocity profile. It is observed that the energy of the mean flow is always decreasing. This is due, first, to transfer of energy to the growing Görtler vortices and, second, to viscous dissipation. But in the time interval during which the energy of the fundamental reaches a maximum and begins to decay, the energy of the mean flow is almost stationary. This suggests that the energy given back to the mean flow by the fundamental balances the energy loss of the mean flow due to viscous dissipation. Therefore the physical explanation for this overshoot phenomenon is that the fundamental initially draws excessive energy from the mean flow and later has to give it back to the mean flow.

Contours of constant streamwise velocity are presented in figure 3 for $T = 3$, 4 and 5. As time progresses, the streamwise velocity profile begins to lose its homogeneity in the spanwise direction and the alternating high-speed and low-speed regions appear as a result of the pumping of low-speed fluid from the wall region into the free stream.

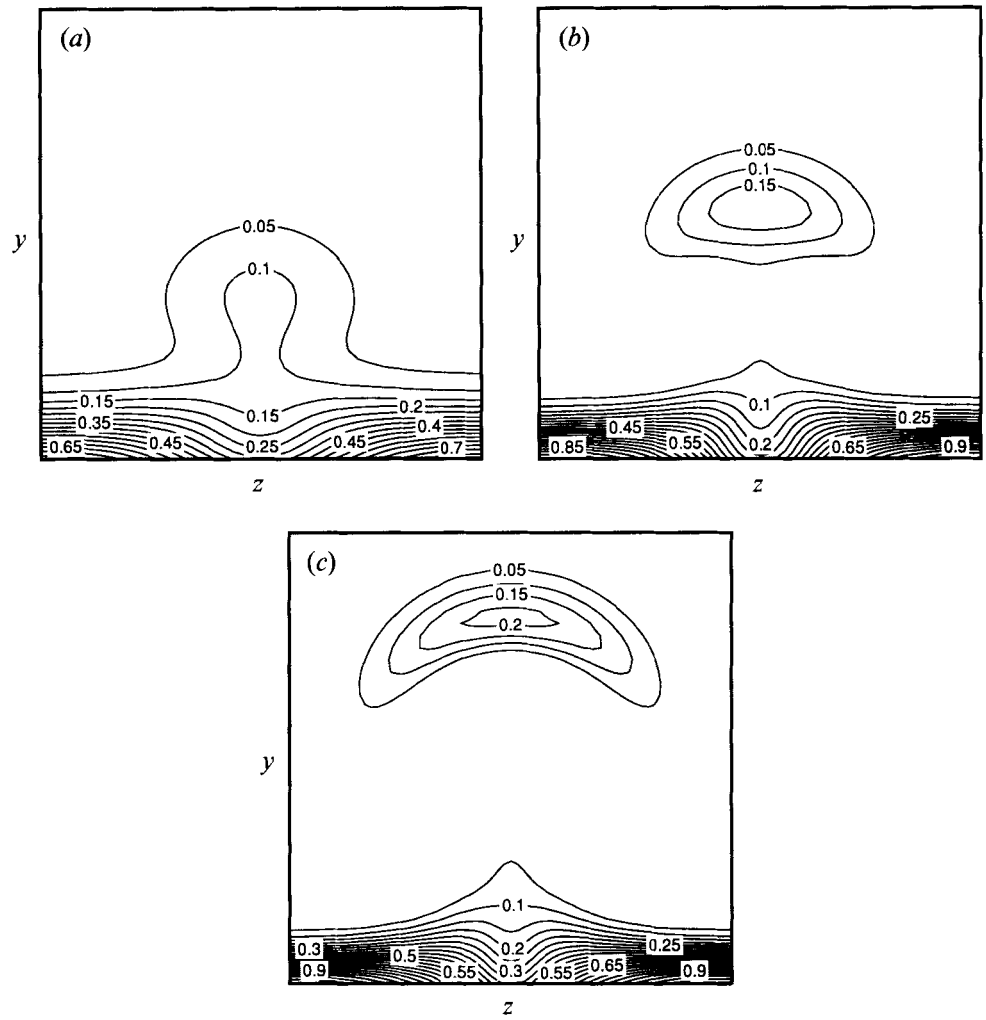

FIGURE 5. Constant $\partial U/\partial y$ contours in the (y, z)-plane for $k_z = 0.5$ and $G = 5$. (*a*) $T = 3$, (*b*) $T = 4$, (*c*) $T = 5$.

The boundary layer is thicker in the upwash region and thinner in the downwash region. As the streamwise vortices intensify, a fully developed mushroom-like contour emerges as seen at $T = 5$ and the streamwise vortices become elongated in the vertical direction and the centres of the vortices move away from the wall. The mushroom-like structures are also observed in the computations of Sabry & Liu (1991) and Liu (1991) and in the experiments by Swearingen & Blackwelder (1987) among others. Peerhossaini & Wesfreid (1988) have observed that vortex centres move vertically when they have grown enough. This shift in position brings the zone of major vortical activity as well as the high-shear region further away from the wall. As mentioned by these authors, this fact could have a major impact on the heat transfer and the skin friction characteristics of the flow. The boundary layer is thicker in the upwash region and thinner in the downwash region.

Corresponding contours of constant $\partial U/\partial z$ and constant $\partial U/\partial y$ are plotted in figures 4 and 5. These plots reveal the existence of regions of high spanwise shear located on either side of the low-speed region and of a region of high vertical shear located at the

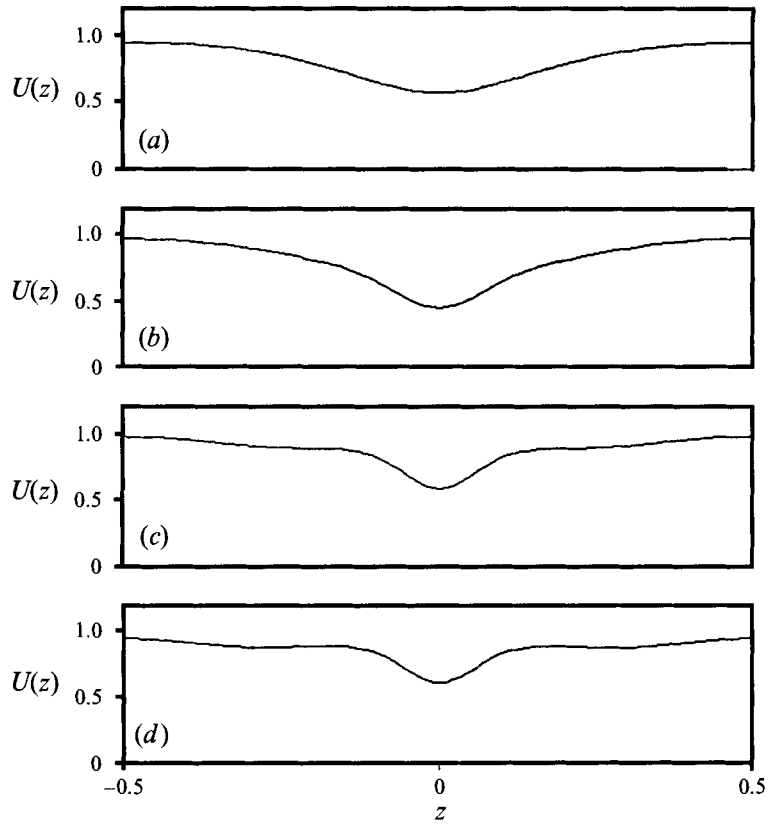

FIGURE 6. $U(z)$ at $y = 4$ for $k_z = 0.5$ and $G = 5$. (*a*) $T = 3$, (*b*) $T = 4$, (*c*) $T = 5$, (*d*) $T = 6$.

upper edge of the boundary layer. These high-shear zones seem to be associated with the production of small-scale oscillatory motion. Shown in figures 6 and 7 are the $U(z)$ profile at $y = 4$ and $U(y)$ profile at $z = 0$, in the low-speed region for $T = 3$, 4, 5 and 6, respectively. At $T = 3$, the inflection point in the spanwise direction distinctly appears and it is accompanied by a relatively large spanwise shear while the inflection point associated with the vertical shear of the $U(y)$ profile is very weak. But at $T = 4$, the $U(y)$ profile also develops a fairly strong inflectional character around $y \sim 8$ while the spanwise shear associated with the inflection point of the $U(z)$ profile becomes very intense on both sides of the low-speed region close to the wall. At $T = 5$, $U(y)$ also becomes highly inflectional. As the inflectional profile develops in the vertical direction, the inflection point begins to move away from the wall with approximately a constant speed. The vertical migration of the inflection point of the $U(y)$ profile is also observed by Swearingen & Blackwelder (1987). At this fully developed stage, both the $U(y)$ and $U(z)$ profiles display multiple inflection points.

The temporal evolution of the destabilizing shear associated with the inflection points is presented in figure 8. The solid line refers to the maximum $\partial U/\partial z$ and the dashed line to $\partial U/\partial y$ at the upper inflection point minus $\partial U/\partial y$ at the lower inflection point. This later quantity measures the amount of unstable spanwise vorticity in the low-speed region. Unstable shear is seen to develop earlier in the spanwise direction than in the vertical direction.

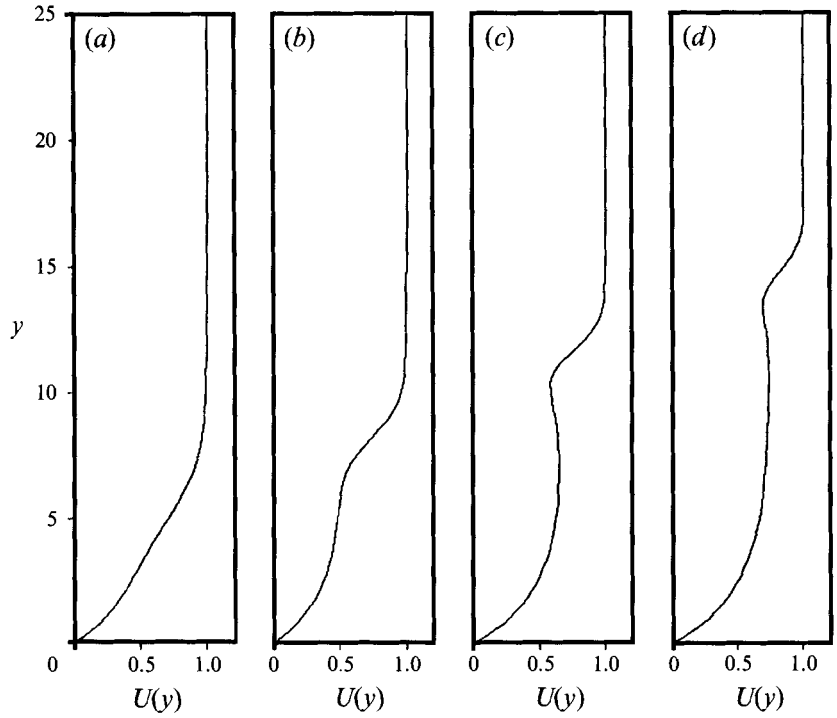

FIGURE 7. $U(y)$ at $z = 0$ (low-speed region) for $k_z = 0.5$ and $G = 5$. (*a*) $T = 3$, (*b*) $T = 4$, (*c*) $T = 5$, (*d*) $T = 6$.

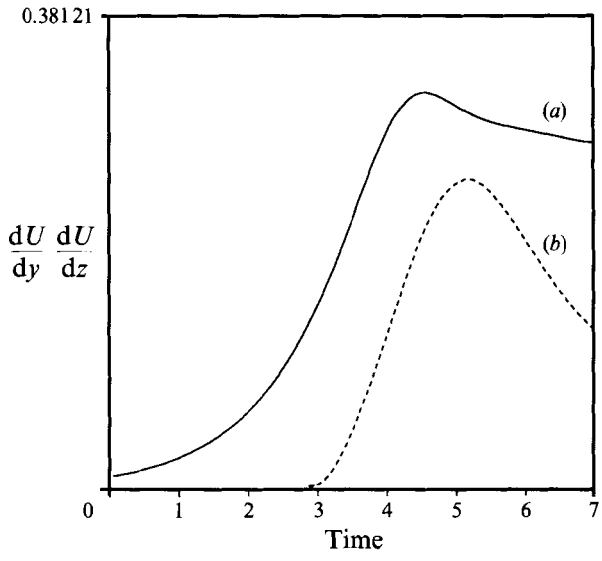

FIGURE 8. Temporal growth of shear components for $k_z = 0.5$ and $G = 5$. (*a*) Maximum $\partial U/\partial z$, (*b*) $\partial U/\partial y$ at upper inflection point minus $\partial U/\partial y$ at lower inflection point.

4.2. *Secondary instability*

The fully inflectional velocity profiles generated by the action of Görtler vortices are unstable on inviscid grounds. We will now present the results of the linear stability analysis of these velocity profiles at $T = 3$, 4 and 5 respectively. The temporal growth

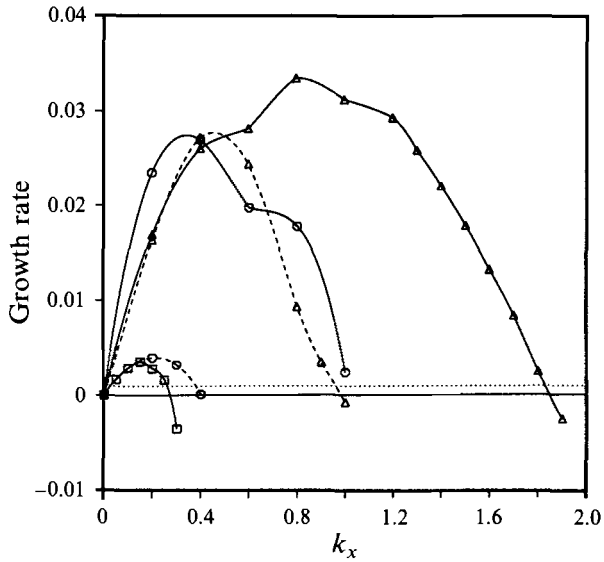

FIGURE 9. Temporal growth rate ω_i versus streamwise wavenumber k_x of the secondary instability. Solid lines refer to the sinuous mode and dashed lines to the varicose mode. □, $T = 3$; ○, $T = 4$; △, $T = 5$. The dotted line is the linear growth rate of the primary Görtler instability. Note that the temporal growth rate of the secondary instability far exceeds that of the primary Görtler instability.

rate ω_i is plotted versus the streamwise wavenumber k_x of the secondary instability in figure 9. The horizontal dotted line represents the linear growth rate of the original Görtler instability. At $T = 3$, the sinuous mode becomes slightly unstable. Its maximum growth rate is about three times that of the Görtler vortices. No unstable varicose mode is found at $T = 3$. At $T = 4$, the sinuous mode becomes highly unstable and it has a broad band of unstable streamwise wavenumbers. The maximum growth rate is far greater than that of the Görtler vortices. Note that the varicose mode is beginning to be slightly unstable with a maximum growth rate slightly larger than that of the sinuous mode at $T = 3$. However, the maximum growth rate of the sinuous mode is about seven times greater than that of the varicose mode. The typical streamwise wavelength of the secondary instability mode is about the same order as the spanwise wavelength of the Görtler vortices. At $T = 5$, both modes are highly unstable. The maximum growth rate of the sinuous mode is slightly greater than that of the varicose mode. Note again that the maximum growth rates for both modes far exceed the Görtler vortex growth rate. The unstable wavenumber bandwidth of the sinuous mode is about twice as broad as that of the varicose mode. The $U(z)$ profile displays, over a single spanwise wavelength, the same shape as a wake. It is known (Drazin & Reid 1981) that for a two-dimensional wake profile, the sinuous or odd mode is more amplified than the varicose or even mode and that its unstable bandwidth is twice as large. Our results at $T = 5$ are therefore qualitatively consistent with those of classical two-dimensional wakes. However, the presence of inflectional profiles in the vertical direction does not allow us to push this analogy any further. The present results are in agreement with Hall & Horseman (1991) whose secondary instability analysis showed that the fastest growing odd (sinuous) mode has a growth rate twice as large as that of the fastest growing even (varicose) mode. Displayed in figure 10 is the plot of the phase speed $c_r = \omega_r/k_x$ versus streamwise wavenumber k_x. The phase speeds of the unstable waves are around 0.7–0.8. These correspond to the streamwise velocity of the

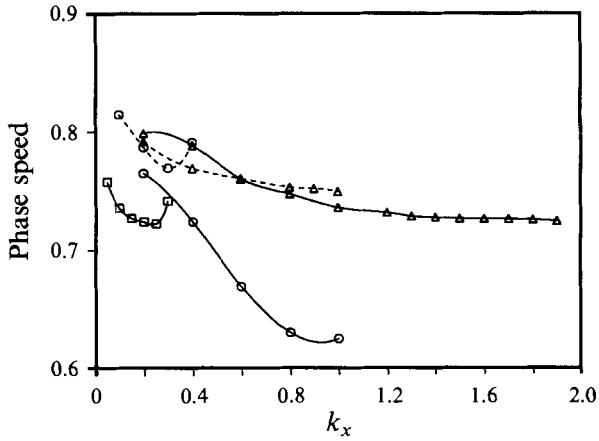

FIGURE 10. Phase speed c_r versus streamwise wavenumber k_x of the secondary instability. Solid lines refer to the sinuous mode and dashed lines to the varicose mode. □, $T = 3$; ○, $T = 4$; △, $T = 5$.

basic flow near the vertical inflection point. At $T = 5$ the phase speed of the sinuous mode and that of the varicose mode are very close to each other for streamwise wavenumbers near 0.2 and 0.6. This phase locking of the two modes may lead to resonance and have a significant effect on their growth in the nonlinear regime.

The respective total growths of the sinuous and varicose are given by

$$\sigma_{sin}(T) = \exp\left[R_E \int_0^T \omega_{i_{sin}}(\tau)\,\mathrm{d}\tau\right], \tag{27}$$

$$\sigma_{var}(T) = \exp\left[R_E \int_0^T \omega_{i_{var}}(\tau)\,\mathrm{d}\tau\right]. \tag{28}$$

Even though the maximum growth rates of the sinuous mode and the varicose mode at $T = 5$ are of the same order of magnitude, the total growth of the sinuous mode, $\sigma_{sin}(T = 5)$, is much larger than that of the varicose mode, $\sigma_{var}(T = 5)$ as a result of the integrated effect. Therefore, for this specific Görtler vortex flow, the transition process appears to be initiated and dominated by the growth of the sinuous mode. In fact, the sinuous mode is often the most frequently observed secondary instability motion as, for instance, in the experiments by Swearingen & Blackwelder (1987). The fact that the temporal growth rates of both modes are much greater than that of the Görtler vortices ensures that the quasi-steady assumption of the basic flow is legitimate. Bippes (1972) has indeed observed that the growth rate of streamwise vortices is relatively small and that a secondary instability mechanism of larger growth rate produces the fluctuations that lead to turbulence. Thus the vortices themselves do not directly break down to turbulence, but set up a flow field which is sensitive to inflectional instabilities with a much higher growth rate.

The constant-r.m.s. contours for the sinuous mode eigenfunction of streamwise wavenumber $k_x = 0.4$ and $T = 5$ are shown in figure 11. The largest velocity component is u_{rms} and the smallest is v_{rms}. Thus for the sinuous mode, the major motion takes place in a horizontal plane. This is in agreement with the conclusions of Blackwelder & Swearingen (1988) stating that the sinuous mode of instability is more successful in producing streamwise and spanwise fluctuations than in producing streamwise and vertical fluctuations. The u_{rms} contour plot for the sinuous mode is very

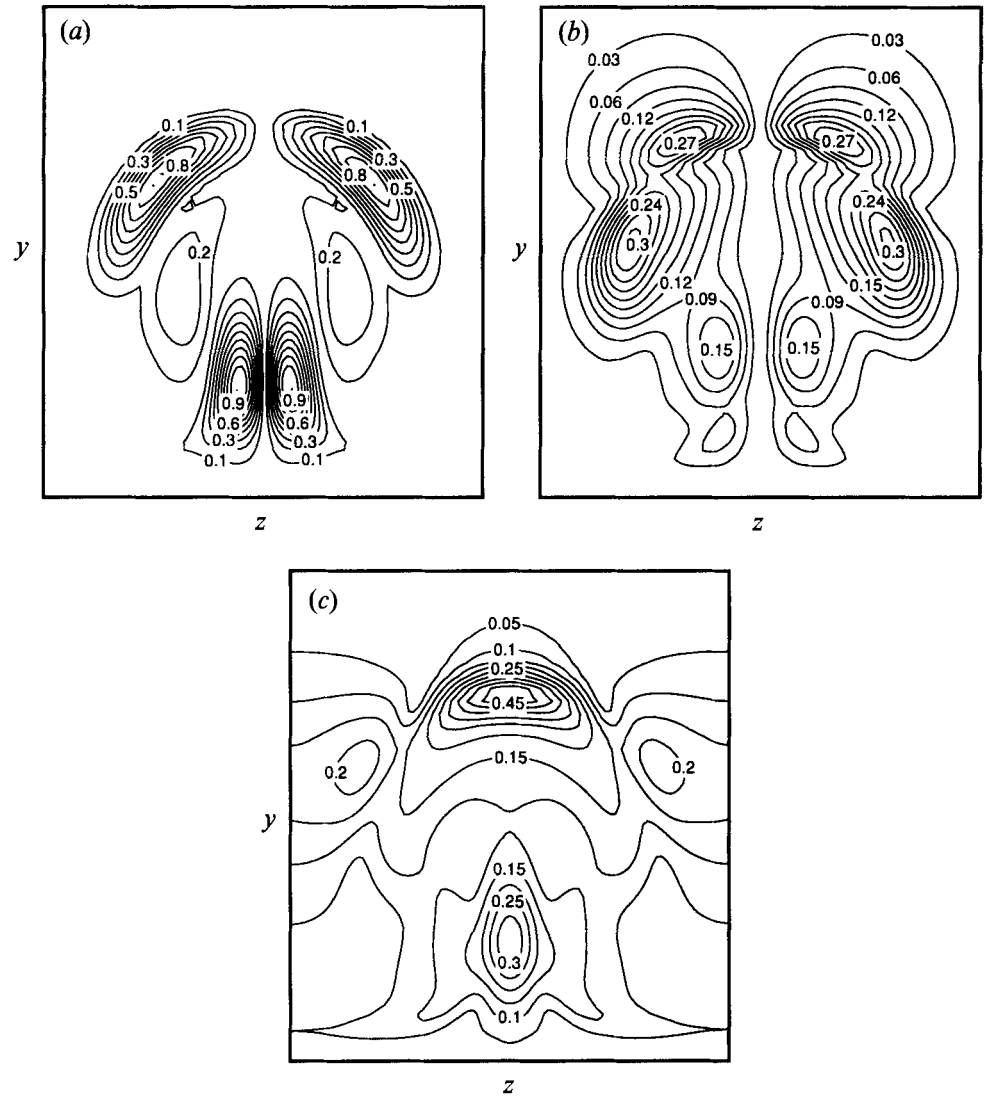

FIGURE 11. Sinuous mode eigenfunction in the (y, z)-plane for $k_x = 0.4$ at $T = 5$. (*a*) u_{rms}, (*b*) u_{rms}, (*c*) w_{rms}. All three components are normalized by the maximum of u_{rms}.

similar to the u_{rms} contour of the direct numerical simulations of Liu (1991), as shown in figure 12, and to the u_{rms} contour plot in the experiments by Swearingen & Blackwelder (1987), as shown in figure 13. Since Liu (1991) solved the full Navier–Stokes equations, the varicose mode as well as the sinuous mode were allowed to evolve. But his solution is mainly documented by the growth of the sinuous mode. This is a strong indication that the dynamics of the sinuous mode play a major role in the transition to turbulence in Görtler flows. It is also noteworthy that the constant-u_{rms} contour plot is extremely well correlated with the constant-$\partial U/\partial z$ contour plot in figure 4. There are two regions, one close to the wall and another near the upper edge of the boundary layer, where the spanwise inflectional shear is very destabilizing. Both regions are unstable at small streamwise wavenumber k_x. However, only the region close to the wall is unstable at high streamwise wavenumber k_x.

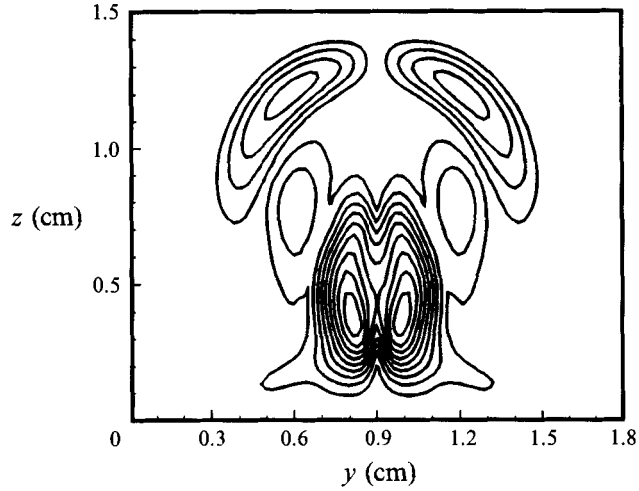

FIGURE 12. Iso-contours of r.m.s. streamwise velocity u_{rms} for secondary motion in the (y, z)-plane (from Liu 1991).

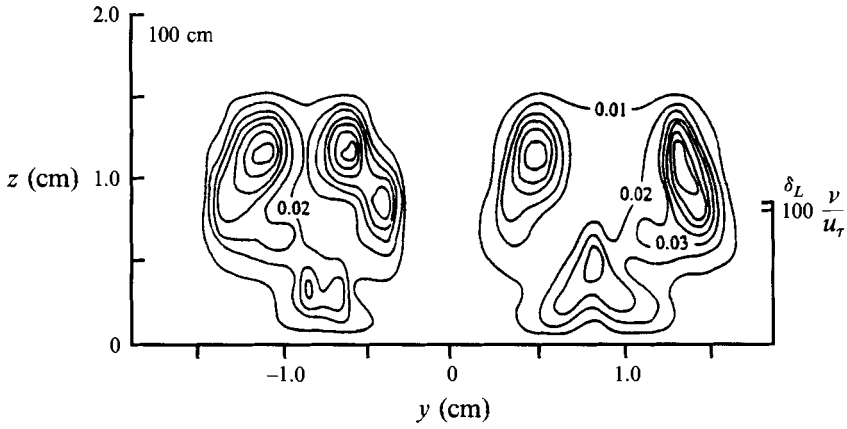

FIGURE 13. Iso-contours of r.m.s. streamwise velocity u_{rms} for secondary motion in the (y, z)-plane (from Swearingen & Blackwelder 1987).

The constant-r.m.s. contours for the varicose mode eigenfunction of streamwise number $k_x = 0.4$ at $T = 5$ are presented in figure 14. Here, u_{rms} is the largest among the three velocity components and w_{rms} is the smallest. Therefore the varicose mode is dominated by up-and-down motion occurring primarily in the vertical plane. The maximum value u_{rms} is located in the region where the shear in the vertical direction is maximum and inflectional. Note that the u_{rms} contours are extremely well correlated with the contours of constant $\partial U/\partial y$ in figure 5. Recall that the varicose mode is damped at $T = 3$ while the sinuous mode is already unstable. The reason for this is that, at $T = 3$, the magnitude of the shear of $U(y)$ at the inflection point is not strong enough to trigger the varicose of instability while $U(z)$ is inflectional enough to trigger the sinuous mode of instability. At $T = 4$, the $U(y)$ profile has also become clearly inflectional and this results in the growth of the varicose mode. Finally at $T = 5$, the inflectional profile in the vertical direction is quite strong as well, and the varicose mode at this stage also becomes highly unstable. The maximum growth rates of the

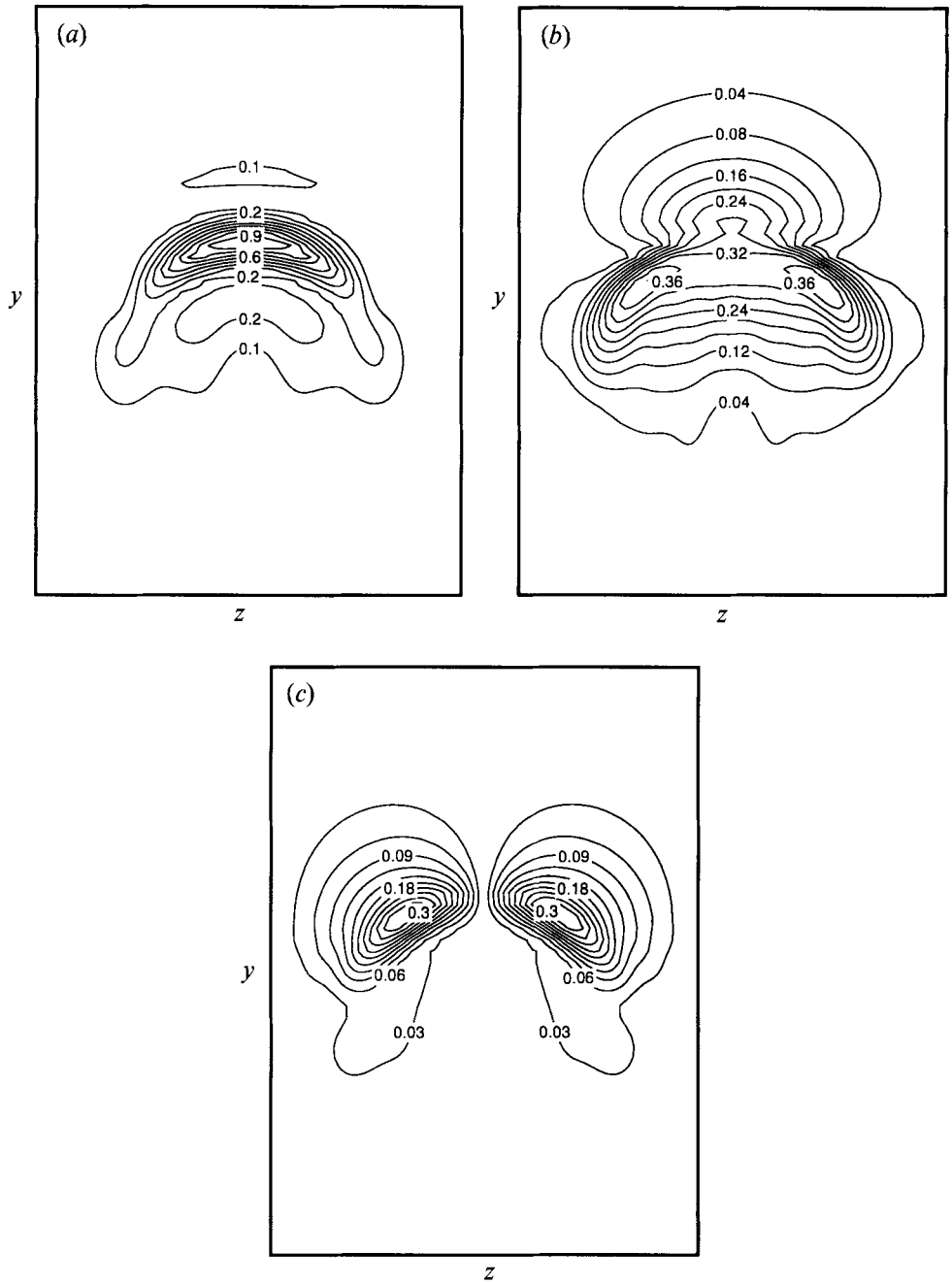

FIGURE 14. Varicose mode eigenfunction in the (y, z)-plane for $k_x = 0.4$ at $T = 5$. (*a*) u_{rms}, (*b*) v_{rms}, (*c*) w_{rms}. All three components are normalized by the maximum of u_{rms}.

sinuous mode at $T = 3$ and of the varicose mode at $T = 4$ are seen to be very comparable. This stems from the fact that the maximum spanwise shear $\partial U/\partial z$ at $T = 3$ and the vertical shear $\partial U/\partial y$ at the upper inflection point minus the vertical shear $\partial U/\partial y$ at the lower inflection point at $T = 4$ are about the same, as indicated in figure 8.

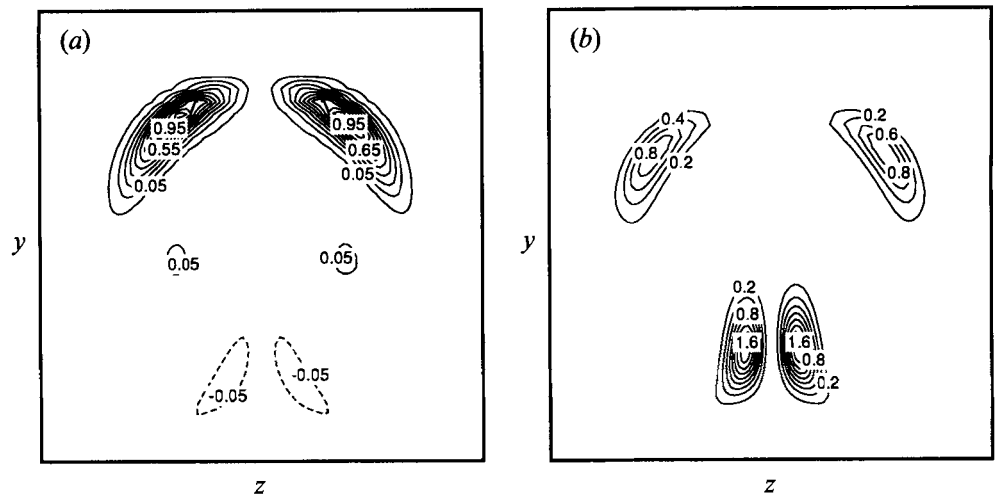

FIGURE 15. Contour plots of kinetic energy production for the sinuous mode at $k_x = 0.4$ and $T = 5$. (*a*) $-(\partial U/\partial y)\overline{uv}$, (*b*) $-(\partial U/\partial z)\overline{uw}$. Contours are normalized by the maximum of $-(\partial U/\partial y)\overline{uv}$.

We define the perturbation kinetic energy as

$$q^2 = \tfrac{1}{2}(u^2+v+w^2). \tag{29}$$

The evolution of the average in the streamwise direction of the kinetic energy is governed by the following equation:

$$\frac{\partial \overline{q^2}}{\partial t} = -\frac{\partial U}{\partial y}\overline{uv} - \frac{\partial U}{\partial z}\overline{uw} - \frac{\partial V}{\partial y}\overline{v^2} - \frac{\partial V}{\partial z}\overline{vw} - \frac{\partial W}{\partial y}\overline{vw} - \frac{\partial W}{\partial z}\overline{w^2} - V\frac{\partial \overline{q^2}}{\partial y} - W\frac{\partial \overline{q^2}}{\partial z} + \frac{1}{R_E}\left\{-\overline{\left(\frac{\partial u}{\partial x}\right)^2}\right.$$
$$\left. -\overline{\left(\frac{\partial v}{\partial x}\right)^2} - \overline{\left(\frac{\partial w}{\partial x}\right)^2} + \overline{\frac{\partial^2 u}{\partial y^2}}u + \overline{\frac{\partial^2 u}{\partial z^2}}u + \overline{\frac{\partial^2 v}{\partial y^2}}v + \overline{\frac{\partial^2 v}{\partial z^2}}v + \overline{\frac{\partial^2 w}{\partial y^2}}w + \overline{\frac{\partial^2 w}{\partial z^2}}w\right\} - \overline{\frac{\partial pv}{\partial y}} - \overline{\frac{\partial pw}{\partial z}}, \tag{30}$$

where

$$\overline{(\cdot)} = \frac{1}{\lambda_x}\int_0^{\lambda_x} (\cdot)\,\mathrm{d}x, \tag{31}$$

and λ_x is the streamwise wavelength. The major portion of the total kinetic energy is produced by the first two terms on the right-hand side because $U = O(1)$ while $V, W = O(R_E^{-1})$. The first term, $-(\partial U/\partial y)\overline{uv}$, represents the production of kinetic energy by the workings of the Reynolds stress $-\overline{uv}$ against the mean vertical shear while the second term, $-(\partial U/\partial z)\overline{uw}$, is the kinetic energy production by the workings of the Reynolds stress $-\overline{uw}$ against the mean spanwise shear. Shown in figure 15 are the contour plots of the kinetic energy production due to these first two terms in the case of the sinuous mode. The major contribution to the total kinetic energy production comes mainly from $-(\partial U/\partial z)\overline{uw}$ and not from $-(\partial U/\partial y)\overline{uv}$ in the upwash region near the wall. This provides strong evidence that the spanwise inflectional velocity profile is the major factor responsible for producing the sinuous mode of instability. In essence, one obtains the equivalent of the sinuous mode in two-dimensional wakes. However, both terms contribute nearly equal amount in the upper region where $\partial U/\partial y$ and $\partial U/\partial z$ are roughly of the same magnitude as shown in figures 4(*c*) and 5(*c*). The opposite is true for the varicose mode as shown in figure 16. The term $-(\partial U/\partial y)\overline{uv}$ completely

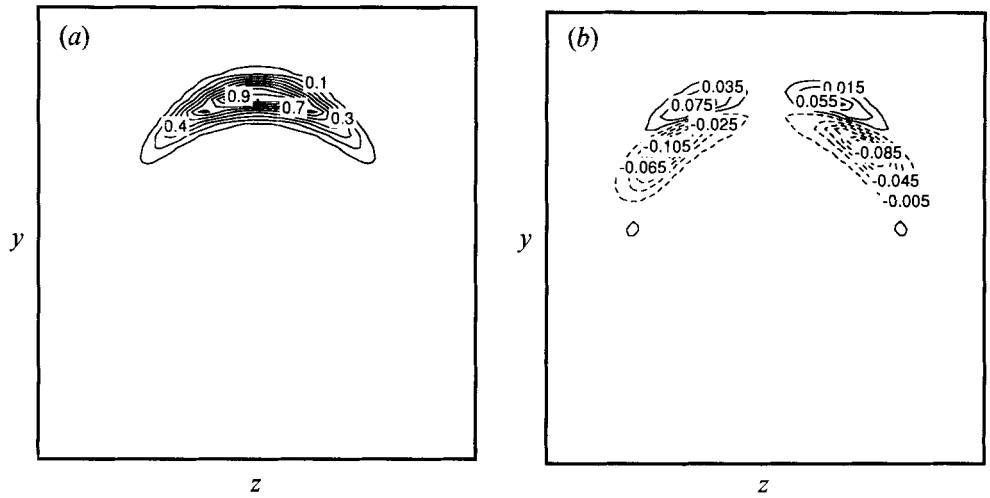

FIGURE 16. Contour plots of kinetic energy production for the varicose mode at $k_x = 0.4$ and $T = 5$. (*a*) $-(\partial U/\partial y)\overline{uv}$, (*b*) $-(\partial U/\partial z)\overline{uw}$. Contours are normalized by the maximum of $-(\partial U/\partial y)\overline{uv}$.

dominates the production of the total kinetic energy. The kinetic energy production by the term $-(\partial U/\partial z)\overline{uw}$ is an order of magnitude smaller. Since the varicose mode draws energy from the unstable shear in the vertical direction which is of the mixing layer type, it is analogous to the Kelvin–Helmholtz instability mode in free shear layers.

In the region close to the wall, the sinuous mode completely dominates and the initial oscillatory motion a fluid particle will experience will be in the (x, z)-plane as the low-speed fluid particle is lifted upward. But as the fluid particle reaches the head of the low-speed region where the varicose mode is strong, it will experience an oscillatory motion in the (x, y)-plane. Therefore smoke wire visualization close to the wall is more likely to reveal the sinuous motion in the (x, z)-plane than the vertically oscillatory motion in the (x, z)-plane.

H. Bippes (1990, personal communication) in a review paper also mentioned two types of secondary instabilities. His conclusion was that the sinuous motion in the (x, z)-plane does not necessarily precede transition but that the horseshoe-type vortices related to the varicose mode do. However, the sinuous motion was observed for small-wavelength Görtler vortices. Our results indicate that the sinuous mode is dominant, which is in line with the experimental observations of Swearingen & Blackwelder (1987). Our findings are also consistent with the direct numerical simulations of the Görtler flow by Liu & Domaradzki (1990). The latter study also demonstrated that the transition to turbulence is initiated in a region characterized by large values of mean spanwise shear $\partial U/\partial z$ rather than by large values of vertical shear $\partial U/\partial y$.

The deciding factor for which mode leads to the breakdown of vortices is probably dependent on the spanwise wavelength of Görtler vortices. For large-wavelength vortices, it is reasonable to think that the varicose mode associated with a large $\partial U/\partial y$ is more likely to dominate the transition process. For small-wavelength vortices, however, we can speculate that the sinuous mode associated with a large $\partial U/\partial z$ will dominate. This is conjectured because the large-wavelength vortices will produce weak spanwise shear while small-wavelength vortices are more likely to produce strong spanwise inflectional shear. Therefore the spanwise wavelength of Görtler vortices could be a critical factor in predicting the dominant mode. Myose & Blackwelder

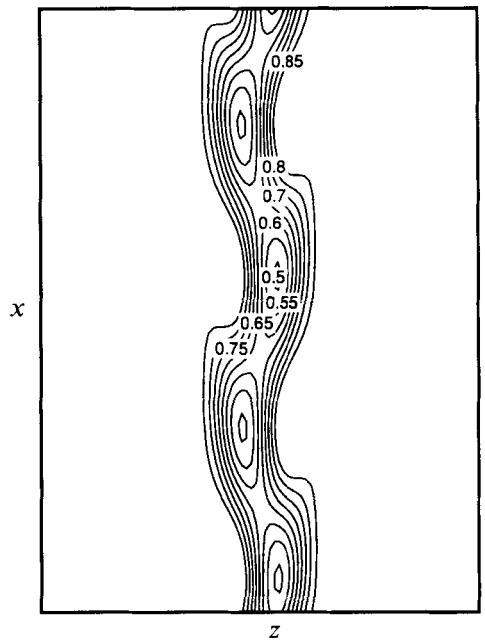

FIGURE 17. Contour plot of the streamwise velocity $(U+u)$ in the (x, z)-plane at $y = 4$ and $T = 5$ for the sinuous mode with the streamwise wavenumber $k_z = 0.4$. Note that this resembles the unstable wake shear layer.

(1991) have also observed that the sinuous or wavy vortex mode is dominant for smaller wavelengths.

The contour plots of the streamwise velocity $(U+u)$ in the horizontal plane at $y = 4$ are displayed for the sinuous mode in figure 17. For clarity, 0.2 is used as the amplitude for the sinuous mode eigenfunction. We see that the sinuous motion of the low-speed region is similar to the initial stage of transition to unsteadiness as described by Swearingen & Blackwelder (1987). Liu (1991) has observed that the growth of the sinuous mode of oscillatory motion in the horizontal plane eventually leads to the breakdown of the curved boundary layer. It also resembles the oscillatory motion of low-speed streaks in turbulent boundary layers. Recently Peerhossaini & Wesfreid (1988) have pointed out that the interface between two neighbouring vortices may oscillate about its stationary mean position. The streamwise rolls bend to the sides, and when the motion is strong enough, they even touch the wall. In figure 18, the contour plots of the total streamwise velocity $(U+u)$ in the cross-stream plane are presented for the sinuous mode at six streamwise stations within a single streamwise wavelength. As the sinuous mode develops, the whole mushroom-like structure oscillates from side to side. Therefore we may conclude that Peerhossaini & Wesfreid (1988) have indeed observed the oscillatory instability motion of the sinuous mode due to the unstable $U(z)$ inflectional velocity profile. The oscillatory motion resulting from the sinuous mode is also very similar to the twisting Dean vortices due to secondary shear instability in curved channel flow as shown in the numerical simulation of Finley, Keller & Ferziger (1988).

Horseshoe-type vortices have been detected in several Görtler flow studies including those by Swearingen & Blackwelder (1987), Aihara & Sonoda (1981), Aihara & Koyama (1981), and Ito (1988). The periodic horseshoe-type vortices which are observed experimentally can be interpreted as arising from the nonlinear evolution of

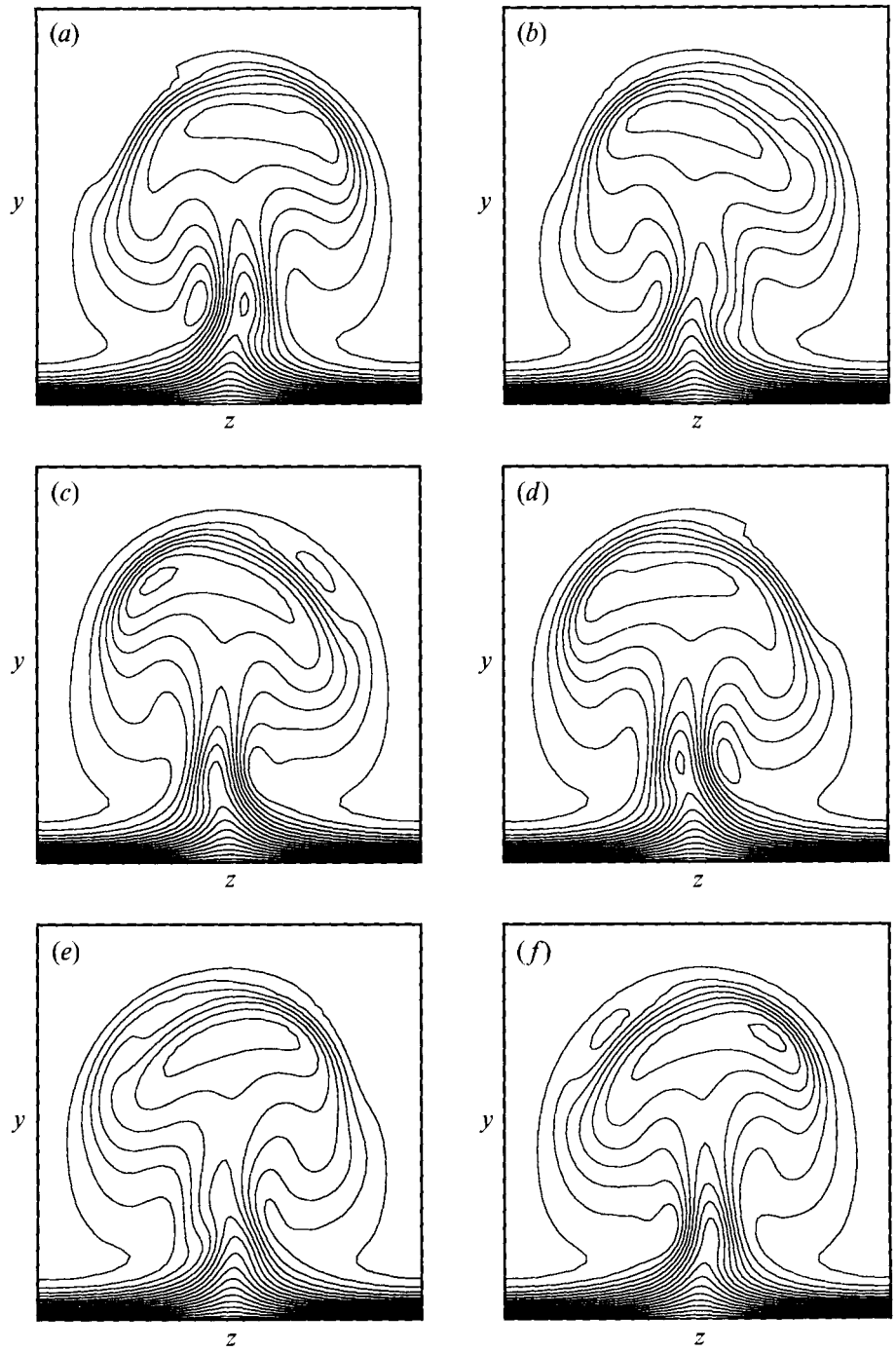

FIGURE 18. Contour plots of the streamwise velocity $(U+u)$ in the (y,z)-plane for the sinuous mode at $k_x = 0.4$ and $T = 5$. (*a*) $x = 0$, (*b*) $x = \lambda_x/6$, (*c*) $x = 2\lambda_x/6$, (*d*) $x = 3\lambda_x/6$, (*e*) $x = 4\lambda_x/6$, (*f*) $x = 5\lambda_x/6$, where λ_x is the streamwise wavelength of sinuous mode.

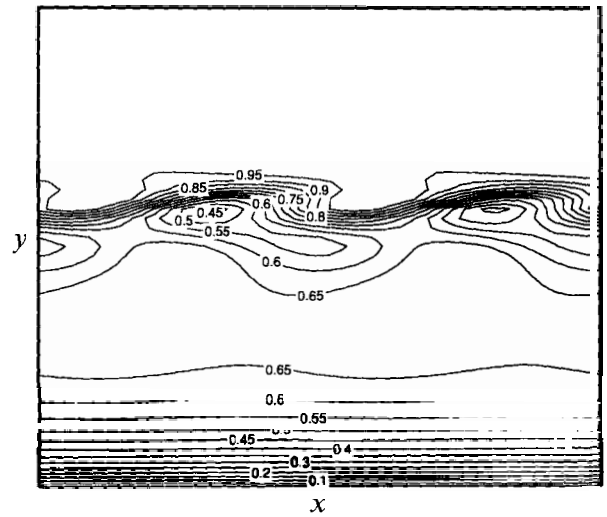

FIGURE 19. Contour plot of the streamwise velocity $(U+u)$ in (x,y)-plane at $z = 0$ (low-speed region) and $T = 5$ for the varicose mode with the streamwise wavenumber $k_z = 0.4$.

the varicose mode. Contour plots of the streamwise velocity $(U+u)$ for the varicose mode in the vertical plane in the upwash region $z = 0$ are displayed in figure 19. For the purpose of illustration, 0.2 is used as the amplitude of the varicose mode eigenfunction. An up-and-down wave motion is observed in the vertical plane around the inflectional region. The head portion of horseshoe-type vortices present in many experiments is probably due to the roll-up of the wavy shear layer similarly to the roll-up of spanwise vortices in two-dimensional free mixing layers as described in detail in Ho & Huerre (1984) among others.

5. Conclusion

Temporally evolving Görtler vortices have been studied by numerically solving the nonlinear Görtler equations. It has been shown that the most important Fourier components participating in the dynamics are the fundamental and the mean flow distortion. These two terms contain most of the perturbation energy. The streamwise velocity profile becomes inflectional both in the spanwise and vertical directions. But the inflectional shear develops earlier in the spanwise direction than in the vertical direction. It is only at a later time that the velocity profile becomes inflectional in the vertical direction with an inflection point located above the low-speed region. Vortices become elongated and move away from the wall as observed experimentally by many investigators including Blackwelder & Swearingen (1988) and Peerhossaini & Wesfreid (1988).

The existence of inflectional velocity profiles had been previously reported in numerous studies, but secondary inflectional instability had been inferred solely on the basis of two-dimensional stability theory. In the present study, the three-dimensional aspects of the linear secondary inflectional instability have been considered and quantified. We emphasize that only the possible exponential growth of secondary perturbations in the linear regime has been examined. We have not attempted to tackle the issue of nonlinear interactions between streamwise vortex structures and instability waves as described in Hall & Smith (1991), or the highly nonlinear events associated with the processes of breakdown and eruptions from the surface in transition to

turbulence on flat-plate boundary layers as reviewed in Smith *et al.* (1991). Our results are in good qualitative agreement with Swearingen & Blackwelder (1987) and with recent results by Liu (1991). We have demonstrated that there exist two instability modes. The sinuous mode is primarily related to the spanwise shear $\partial U/\partial z$ while the varicose mode is related to the vertical shear $\partial U/\partial y$. Since the spanwise inflectional profile develops before the vertical inflectional profile, the sinuous mode becomes unstable earlier than the varicose mode and possibly dominates the transition process. These secondary instability modes have a streamwise wavelength comparable to the Görtler wavelength. The largest contribution to kinetic energy production comes from $-(\partial U/\partial z)\overline{uw}$ for the sinuous mode and from $-(\partial U/\partial y)\overline{uv}$ for the variose mode. The sinuous mode induces motion that is observed close to the wall region and it is analogous to the dominant instability mode in plane wakes. The horseshoe-type vortices detected experimentally could possibly originate from the roll-up of spanwise vortices triggered by the varicose mode. This nonlinear mechanism is similar to the roll-up of spanwise vortices in mixing layers.

The authors wish to thank Professors R. F. Blackwelder, A. J. Domaradzki and L. G. Redekopp for helpful discussions and comments. This study is largely based on the first author's PhD thesis (Park 1990). The secondary instability portion was presented in the Colloquium on Görtler Vortex Flows, EUROMECH 261 at Université de Nantes, France (Park & Huerre 1990). This work was mainly supported by ONR-URI N0001486-K-0679 and a Powell Foundation Fellowship.

REFERENCES

AIHARA, Y. 1979 Görtler vortices in the nonlinear region. In *Recent Developments in Theoretical and Experimental Fluid Mechanics*, pp. 331–338. Springer.

AIHARA, Y. & KOYAMA, H. 1981 Secondary instability of Görtler vortices – formation of periodic three-dimensional coherent structure. *Trans. Japan Soc. Aero. Astron. Sci.* **24**, 78–94.

AIHARA, Y. & SONODA, T. 1981 Effects of pressure gradient on the secondary instability of Görtler vortices. *AIAA*-81-0197.

ALFREDSSON, P. H. & MATSSON, O. J. E. 1990 The effect of curvature and rotation on the stability of channel flow. In *Colloquium on Görtler Vortex Flows, Synopsis of Contributions*. EUROMECH 261, Université de Nante, France.

BASSOM, A. P. & SEDDOUGUI, S. O. 1990 The onset of three-dimensionality and time dependence on Görtler vortices: neutrally stable wavy modes. *J. Fluid Mech.* **220**, 661–672.

BIPPES, H. 1972 Experimentelle Untersuchung des laminar-turbulenten Umschlags an einer parallel angeströmten könkaven Wand. *Heidelberger Akademie der Wiss. Math. Naturw. Klasse*, pp. 103–180.

BLACKWELDER, R. F. & SWEARINGEN, J. D. 1988 The role of inflectional velocity profiles in wall bounded flows. In *Near-Wall Turbulence* (ed. S. J. Kline). Hemisphere.

DRAZIN, P. G. & REID, W. H. 1981 *Hydrodynamic Stability*. Cambridge University Press.

FINLEY, W. H., KELLER, J. B. & FERZIGER, J. H. 1988 Instability and transition in curved channel flow. *J. Fluid Mech.* **194**, 417–456.

FLORYAN, J. M. & SARIC, W. S. 1979 Stability of Görtler vortices in boundary layers. *AIAA J.* **20**, 316–324.

GÖRTLER, H. 1940 Über eine dreidimensionale Instabilität laminarer Grenzschichten an konkaven Wänden. *Nachr. Ges. Wiss. Göttingen, Math. Phys. Klasse, Neue Folge* **2**, 1–26.

HALL, P. 1982*a* On the nonlinear evolution of Görtler vortices in growing boundary layers. *J. Inst. Maths Applics.* **29**, 173–196.

HALL, P. 1982*b* Taylor–Görtler instabilities in fully developed or boundary layer flows: linear theory. *J. Fluid Mech.* **124**, 475–494.

HALL, P. 1983 The linear development of Görtler vortices in growing boundary layers. *J. Fluid Mech.* **130**, 41–58.

HALL, P. 1988 The nonlinear development of Görtler vortices in growing boundary layers. *J. Fluid Mech.* **193**, 243–266.

HALL, P. & HORSEMAN, N. J. 1991 The linear inviscid secondary instability of longitudinal vortex structures in boundary layers. *J. Fluid Mech.* **232**, 357–375.

HALL, P. & LAKIN, W. D. 1988 The fully nonlinear development of Görtler vortices in growing boundary layers. *Proc. R. Soc. Lond.* A **415**, 421–444.

HALL, P. & SEDDOUGUI, S. O. 1989 On the onset of three-dimensionality and time-dependence in Görtler vortices. *J. Fluid Mech.* **204**, 405–420.

HALL, P. & SMITH, F. T. 1991 On strongly nonlinear vortex/wave interactions in boundary-layer transition. *J. Fluid Mech.* **227**, 641–666.

HO, C. M. & HUERRE, P. 1984 Perturbed free shear layers. *Ann. Rev. Fluid Mech.* **16**, 365–424.

ITO, A. 1980 The generation and breakdown of longitudinal vortices along a concave wall. *J. Japan Soc. Aerospace Sci.* **28**, 327–333.

ITO, A. 1988 On the relation of horseshoe-type vortices and fluctuating flows. *J. Japan Soc. Aerospace Sci.* **36**, 274–279.

LIU, W. 1991 Direct numerical simulation of transition to turbulence in Görtler flow. PhD thesis, University of Southern California, Department of Aerospace Engineering.

LIU, W. & DOMARADZKI, J. A. 1990 Direct numerical simulation of transition to turbulence in Görtler flow. *AIAA*-90-0114.

MYOSE, R. Y. & BLACKWELDER, R. F. 1991 Controlling the spacing of streamwise vortices on concave walls. *AIAA J.* **20**, 1901–1905.

PARK, D. S. 1990 The primary and secondary instabilities of Görtler flow. PhD thesis, University of Southern California, Department of Aerospace Engineering.

PARK, D. S. & HUERRE, P. 1990 The secondary instability of the nonlinearly developing Görtler vortices. In *Colloquium on Görtler Vortex Flows, Synopsis of Contributions.* EU-ROMECH 261, Université de Nantes, France.

PEERHOSSAINI, H. 1984 On the subject of Görtler vortex. In *Cellular Structures in Instabilities* (ed. J. E. Wesfreid & S. Zaleski), pp. 376–384. Springer.

PEERHOSSAINI, H. & WESFREID, J. E. 1988 On the inner structure of streamwise Görtler rolls. *Intl J. Heat Fluid Flow* **9**, 12–18.

RAYLEIGH, LORD 1916 On the dynamics of revolving fluids. *Proc. R. Soc. Lond.* A **93**, 148–154.

SABRY, A. S. & LIU, J. T. C. 1991 Longitudinal vorticity elements in boundary layers: nonlinear development from initial Görtler vortices as a prototype problem. *J. Fluid Mech.* **231**, 615–663.

SMITH, C. R., WALKER, J. D. A., HAIDARI, A. H. & SOBRUN, U. 1991 On the dynamics of near-wall turbulence. *Phil. Trans. R. Soc. Lond.* A **336**, 131–175.

SWEARINGEN, J. D. & BLACKWELDER, R. F. 1987 The growth and breakdown of streamwise vortices in the presence of a wall. *J. Fluid Mech.* **182**, 255–290.

TAYLOR, G. I. 1923 Stability of a viscous liquid contained between two rotating cylinders. *Phil. Trans. R. Soc. Lond.* A **223**, 289–343.

WINOTO, S. H. & CRANE, R. I. 1980 Vortex structure in laminar boundary layers on a concave wall. *Intl J. Heat Fluid Flow* **2**, 221–231.